Chapter 3

ROBUST SPIN ICE FREEZING IN MAGNETICALLY FRUSTRATED $Ho_2Ti_2O_7$ AND CRYSTAL FIELD-PHONON COUPLING

3.1 Introduction

Among pyrochlore oxides, magnetic pyrotitanates lie in the specific class of spin ice systems and are arguably the most promising materials. The ultimate goal will require both a thorough understanding of their structure and strategy to synthesize new materials. In titanates, magnetic exchange (J_{nn}) and dipolar interaction (D_{nn}) between the nearest neighbor spins decide the low-temperature magnetic properties. The ratio of dipolar and exchange coupling constants decides the stability regime of spin ice materials ($J_{nn}/D_{nn} > -0.91$; the dominance of dipolar interaction). Below this value system acquires an ordered state ($J_{nn}/D_{nn} < -0.91$; the dominance of exchange interaction) at lower temperature following a transition to Q = 0 antiferromagnetic state where spins follow "all in-all out" configuration in tetrahedron [60]. Zhou *et al.* presented the theoretical and experimental comparison of magnetic interaction parameters of two sets of pyrochlores spin-ices $Ho_2X_2O_7$ and $Dy_2X_2O_7$ (X = Sn, Ti & Ge) respectively that depicts the effect of the application of chemical pressure [60]. The changes in chemical potential led to the variation in lattice parameters as well as the magnetic interaction parameter, as shown in **Table 3.1.**

Table 3.1 Lattice parameters and magnetic-interaction parameters for six pyrochlore spin-ices. [60]

Compound	*a (Å)*	*θ_{CW} (K)*	*D_{nn} (K)*	*C_{peak} (J/mol$_{Ho,Dy}$. K)*	*T_{peak} (K)*	*J_{nn}/D_{nn} (K)*	*J_{eff}*
$Ho_2Sn_2O_7$	10.37	1.8	2.17	2.41	1.65	-0.26	1.61
$Ho_2Ti_2O_7$	10.10	1.9	2.35	2.61	1.75	-0.27	1.72
$Ho_2Ge_2O_7$	9.90	0.06	2.50	3.04	1.70	-0.35	1.63
$Dy_2Sn_2O_7$	10.40	1.7	2.15	2.65	1.20	-0.46	1.16
$Dy_2Ti_2O_7$	10.10	0.5	2.35	2.72	1.25	-0.49	1.20
$Dy_2Ge_2O_7$	9.93	0.0	2.47	3.17	0.828	-0.73	0.67

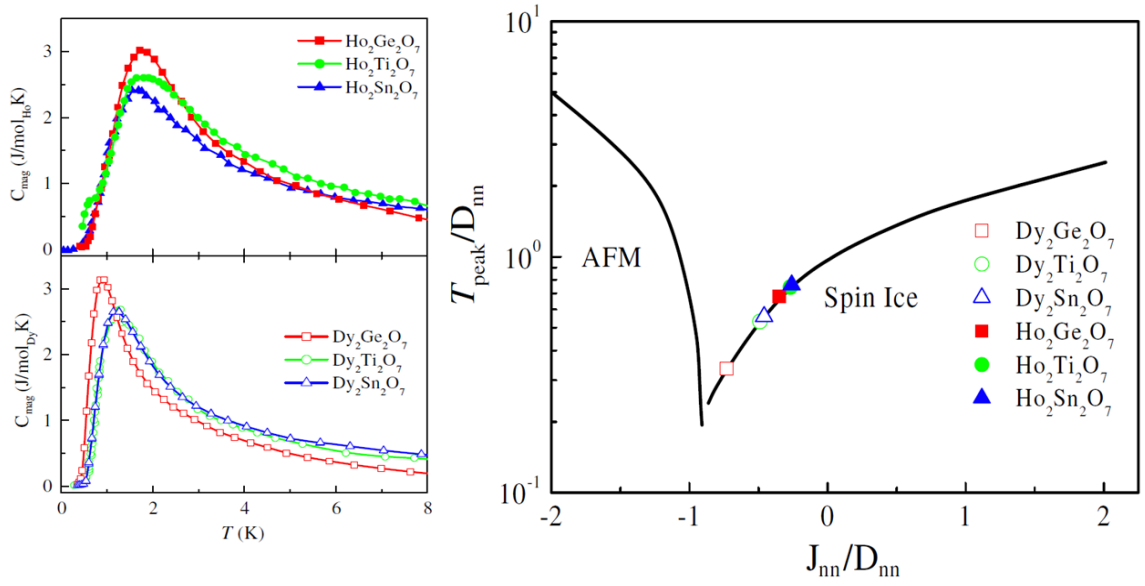

Figure 3.1 (a) Dependence of the specific heat peak position on T. (b) Dependence of T_{peak}/D_{nn} on J_{nn}/D_{nn} ratio. The open symbols are experimental results, and the solid lines are the theoretical calculations from the dipolar spin-ice model.[60]

The variation in the magnetic interaction due to chemical pressure effect is calculated from the specific heat peak position and it drives the system towards the antiferromagnetic phase boundary from the spin-ice region, as shown in **Figure 3.1**. The Hamiltonian accounting for the interaction between magnetic ions is based upon the dipolar spin ice model (DSIM) and is given as equation 1.36 in chapter 1 . By varying the complex dipolar (D_{nn}) and exchange

interaction (J_{nn}) within this 'spin ice Hamiltonian,' the spin ice state could initiate long-range ordering in $Ho_2Ti_2O_7$. The separation between the magnetic dipoles and the degree of their mutual alignment controls the interactions responsible for spin relaxation behavior in these systems, and it can be tuned through the induced structural distortion due to chemical pressure. The dominance of any of these particular interactions, namely crystal field, dipolar, and exchange, varies with temperature. We focused on Ge^{4+} substitution at Ti^{4+} site in $Ho_2Ti_2O_7$, creating positive chemical pressure in the $Ho_2Ti_2O_7$ matrix. This chapter presents structural analysis and detailed magnetic studies using ac susceptibility, M-T, and M-H measurements.

3.2 Structural analysis

$Ho_2Ti_2O_7$ spin ice exhibits cubic structure having space group $Fd\bar{3}m$. $Ho_2Ti_2O_6O'$ is the preferable formula with an anti-prismatic arrangement of the six oxygen atoms around the central Ho^{3+} ion. The plane is transverse to O'-Ho-O' linear axis. A strong axial symmetry is exhibited along the [111] axis, which is the direction containing two O' atoms connected through the shared Ho^{3+} atom of the adjacent tetrahedra. Both the atomic arrangements showing the Ho-O' unit and the symmetry around the [111] axis of this connection is shown in **Figure 3.2** and **Figure 3.3**. The O'^{2-} ions are responsible for the anti-prismatic character of the D_{3d} site symmetry of the Ho^{3+} ion. It is a form of manifestation of the Stark effect that considers the effect of negative charge of these oxygen atoms on rare earth (4f electronic configuration), and it decides the quantum states of Ho^{3+} single ion [58].

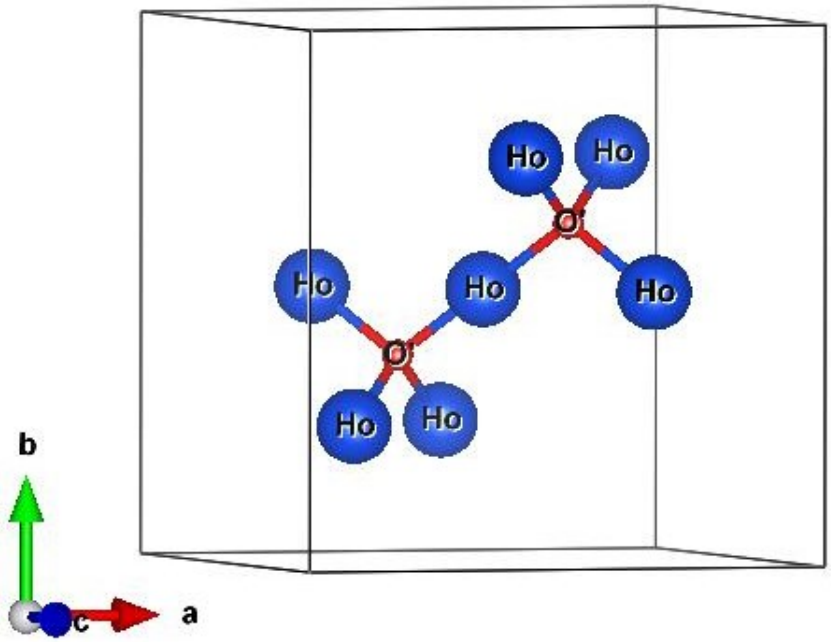

Figure 3.2 A part of pyrochlore lattice containing two O' atoms connected through the shared Ho^{3+} atom of the adjacent tetrahedra.

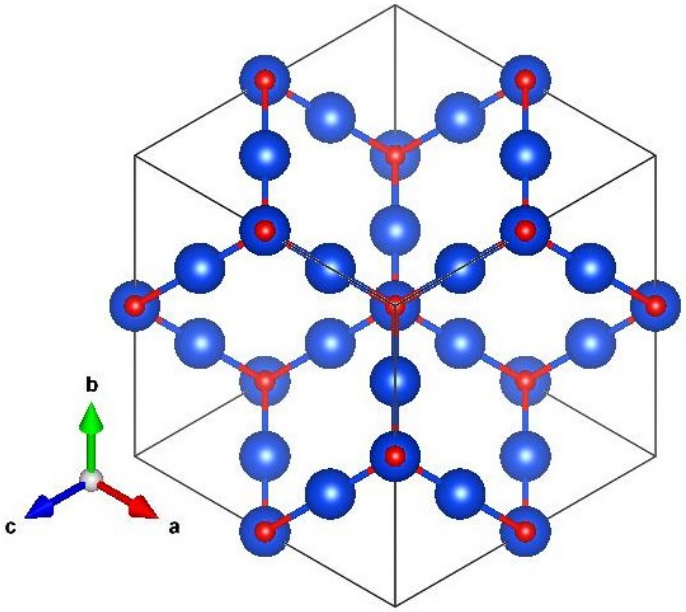

Figure 3.3 The projection of pyrochlore lattice along [111] direction highlighting the strong axial symmetry containing the O' oxygen ions (red spheres) and magnetic Ho^{3+} (blue spheres) ions only.

3.2.1 Rietveld refinement of HRXRD pattern of $Ho_2Ge_xTi_{2-x}O_7$

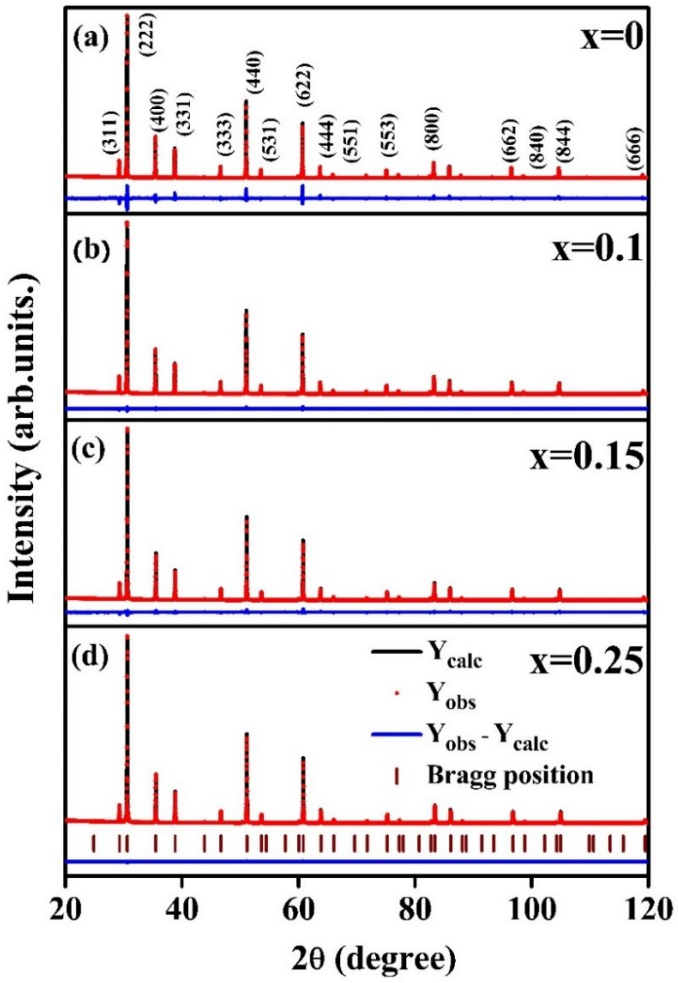

Figure 3.4 Room temperature high resolution X-ray diffraction (HRXRD) pattern of $Ho_2Ge_xTi_{2-x}O_7$ for (a) x = 0 (b) x= 0.1 (c) 0.15 (d) 0.25.

Figure 3.4 shows the Rietveld refinement of the room temperature HRXRD pattern of $Ho_2Ge_xTi_{2-x}O_7$ (from x= 0 to x = 0.25). All the peaks in this pattern are due to the pyrochlore structure having space group $Fd\bar{3}m$. The phase purity is confirmed from the absence of any impurity peak present in the samples.

3.2.2 Role of positive chemical pressure on the structure

The effect of increased chemical pressure could be seen in **Figure 3.5,** which shows the shift of (222), (440), (622), and (662) peaks towards higher theta value with an increase in x from 0 to 0.25 in $Ho_2Ge_xTi_{2-x}O_7$.

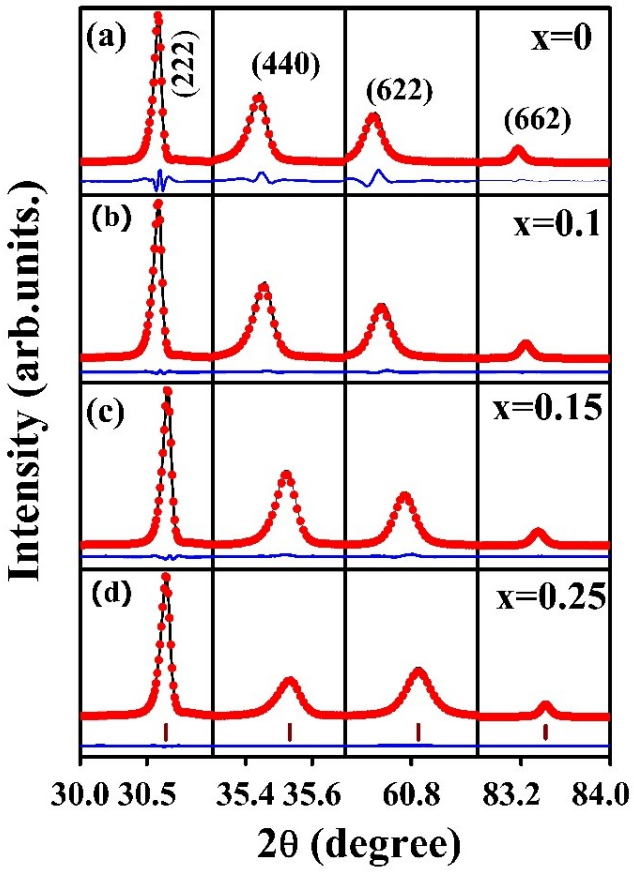

Figure 3.5 Room temperature high resolution x-ray diffraction data (HRXRD) indicating the shift of (222), (440), (622) and (662) peaks towards higher Q value and with increase in chemical pressure for (a) x = 0 (b) x = 0.1 (c) x = 0.1 (d) x = 0.25) in $Ho_2Ge_xTi_{2-x}O_7$.

It clearly indicates shrinkage in lattice parameter with increasing chemical pressure in $Ho_2Ti_2O_7$ matrix. The sequential reduction in lattice parameter (obtained from Rietveld refinement) is shown pictorially in **Figure 3.6**. The crystallographic parameters of $Ho_2Ge_xTi_{2-}$

$_xO_7$ as obtained from the Reitveld refinement of HRXRD data at 300 K are shown in **Table 3.2** along with the other details. The lattice volume, Ho-O, Ho-O' & Ho-Ho (bond length) and angular separation between O-Ho-O' (bond angle) decreases with increasing chemical pressure, along with the other systematic changes.

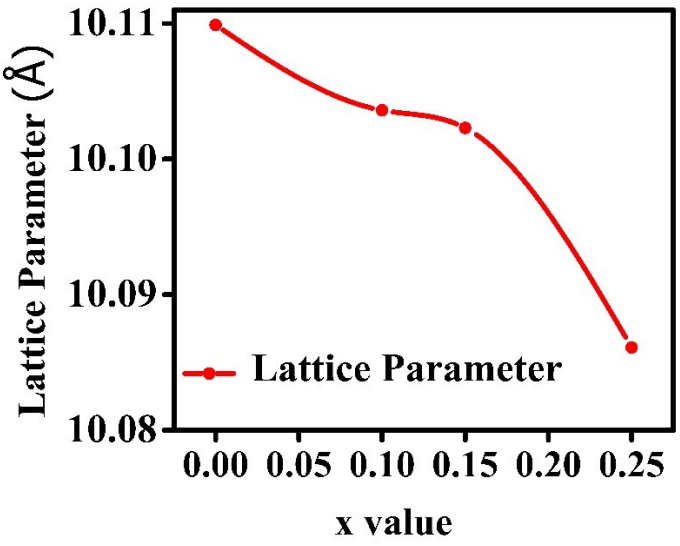

Figure 3.6 Variation of lattice parameter with x for $Ho_2Ge_xTi_{2-x}O_7$.

Table 3.2 Bond length and bond angles of $Ho_2Ge_xTi_{2-x}O_7$ (x = 0, 0.1, 0.15 & 0.25) series obtained from Rietveld refinement of HRXRD data.

x	Lattice Parameter (Å)	Refinable Parameter (x,0,0)	Bond length (Å)				Bond angle (°)		
			Ho-O	Ho-O'	Ti-O	Ho-Ho	O-Ho-O'	O-Ho-O	O-Ti-O
0	10.1099(1)	0.3308(3)	2.4740(3)	2.1889(0)	1.9650(2)	3.5744(0)	79.01(6)	63.55(4)	83.04(1)
0.1	10.1036(1)	0.3310(1)	2.4610(3)	2.1875(0)	1.9710(2)	3.5722(1)	78.72(6)	63.73(4)	82.45(1)
0.15	10.1023(1)	0.3325(1)	2.4599(1)	2.1872(0)	1.9709(1)	3.5717(0)	78.72(1)	63.73(1)	82.44(1)
0.25	10.0861(1)	0.3327(1)	2.4552(1)	2.1837(0)	1.9682(1)	3.5660(3)	78.79(6)	63.75(1)	82.59(1)

3.3 Magnetic properties

To study the magnetic properties after Ge inclusion upto 12.5%, the temperature dependent magnetization, magnetic field dependent magnetization and temperature dependent ac-usceptibility were carried out and are discussed in 3.3.1, 3.3.2 and 3.3.3, respectively.

3.3.1 Temperature dependent magnetization

Temperature dependence magnetization (M-T) measurement for $Ho_2Ge_xTi_{2-x}O_7$ (x = 0, 0.1, 0.15 and 0.25) bulk sample has been performed between (2-200) K at an applied field of 100 Oe and 1000 Oe.

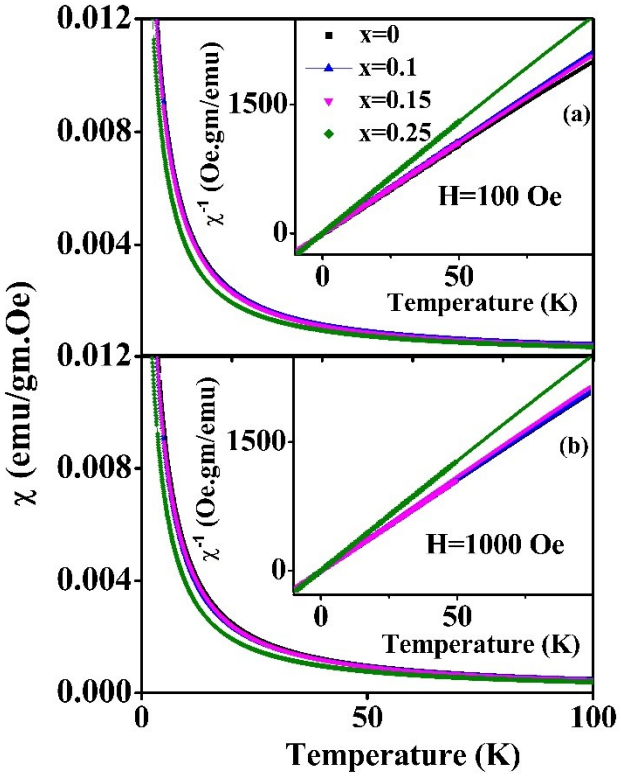

Figure 3.7 Temperature dependence of dc susceptibility curve of $Ho_2Ge_xTi_{2-x}O_7$ (x = 0, 0.1, 0.15 and 0.25) samples in the range of (2-200) K for (a) H = 100 Oe (b) and 1000 Oe. The inset shows the corresponding inverse susceptibility curve obtained from dc χ for ZFC data.

Data shows no difference in the FC (field cooling) and ZFC (zero-field cooling) magnetisation measurement, indicating no evidence of any spin-glass freezing down to 2 K. **Figure 3.7 (a)** & **Figure 3.7 (b)** shows dc susceptibility plot at an applied field of H=100 Oe and 1000 Oe respectively. It increases monotonously, similar to paramagnetic behaviour, indicating no ordering or any transition related to spin freezing till 2 K.

The plot is fitted using the Curie-Weiss equation in three different linear temperature ranges of (10-20) K, (15-25) K, and (20-30) K; using

$$\chi = N_A\mu^2_{eff}/3k_B(T-\theta_{cw}) \quad (3.1)$$

where, θ_{cw} is the Curie Weiss temperature, μ_{eff} is the effective magnetic moment, k_B is the Boltzmann constant, and N_A is the Avogadro number. [61].

A typical fitted χ^{-1} vs T plot for the range of (10-20) K is shown in insets of **Figure 3.7 (a)** & **Figure 3.7 (b).** For the fitting temperature range (15-25) K, θ_{cw} decreases from 0.36 K to -0.03 K for H = 100 Oe, and from 0.09 K to -0.40 K for H = 1000 Oe. Similarly, for temperature range (20-30), θ_{cw} reduces from 0.68 K to 0.22 K (H = 100 Oe) and from 0.72 K to 0.21 K (H = 1000 Oe).. Similar trend in θ_{cw} was obtained with increase in positive chemical pressure. The values are summerized in **Table 3.3.**

Table 3.3 Value of dipolar interaction and Curie Weiss temperature for $Ho_2Ge_xTi_{2-x}O_7$ (x = 0, 0.1, 0.15 & 0.25) sample series obtained from Curie Weiss fitting at 100 and 1000 Oe. The values in bracket represent the error.

Compound	θ_{cw} (K); H=100 Oe	θ_{cw} (K); H=1000 Oe	θ_{cw} (K); H=100 Oe	θ_{cw} (K); H=1000 Oe	θ_{cw} (K); H=100 Oe	θ_{cw} (K); H=1000 Oe	D_{nn} (K); Dipolar interaction
	Fitting range = (10-20)K		Fitting range = (15-25)K		Fitting range = (20-30)K		
$Ho_2Ge_2O_7$	0.33(0.09)	0.25(0.08)	0.36(0.13)	0.09(0.06)	0.68(0.34)	0.72(0.43)	2.2725
$Ho_2Ti_{1.9}Ge_{0.1}O_7$	0.14(0.07)	0.09(0.06)	0.34(0.25)	0.04(0.10)	0.40(0.26)	0.69(0.30)	2.2767
$Ho_2Ti_{1.85}Ge_{0.15}O_7$	0.14(0.08)	0.11(0.08)	0.25(0.08)	0.02(0.10)	0.43(0.22)	0.22(0.11)	2.2776
$Ho_2Ti_{1.75}Ge_{0.25}O_7$	-0.04(0.03)	-0.02(0.01)	-0.03(0.01)	-0.40(0.07)	0.22(0.13)	0.21(0.09)	2.2886

The mid range values of Curie-Weiss temperature for the temperature range of (10-20) K has been considered for further disscussion. θ_{cw} reduces to 0.14 K (x=0.15) from 0.33 K (x=0) with the increase in chemical pressure in $Ho_2Ti_2O_7$ matrix for an applied field of 100 Oe. θ_{cw} further decreases to a negative value of -0.04 K with the increase in x to 0.25 for $Ho_2Ge_xTi_{2-x}O_7$. A similar trend is followed in the value of θ_{cw} for an increased applied field of 1000 Oe, with slightly decreased values. For H=1000 Oe, θ_{cw} decreases from 0.2534 K (x=0) to -0.0141 K (x=0.25).

This tendency of reduction in the value of θ_{cw} with an increase in chemical pressure is indicative of the increase in AFM interaction though overall interaction remains FM pertaining to spin ice configuration.

Systematic decrease in Ho-Ho separation (r_{nn}) from 3.5744(0) Å (x=0) to 3.5660(3) Å (x=0.25) at 300 K (as shown in **Table 3.2**) indicates very insignificant increment in dipolar interaction (D_{nn}). Nearest neighbor dipolar interaction energy between Ho^{3+} ions is calculated using a simple formula given by *Stöter et al.* as [21]

$$D_{nn} = 5/3(\mu_\circ/4\pi)\mu^2/r^3_{nn} \quad (3.2)$$

We observe a minimal increment in D_{nn} from 2.2725 K (x=0) to 2.2886 (x=0.25). The numerical values of D_{nn} are listed in **Table 3.3.**

Dipolar FM interaction remains almost constant, but a reduction in θ_{cw} indicates an enhancement in Ho-Ho AFM exchange interaction (J_{nn}) with an increase in x in $Ho_2Ge_xTi_{2-x}O_7$. Using the value of the magnetic moment of Ho^{3+} ion to be 10 μ_B and r_{nn} = 3.6 Å *Zhou et al.* has calculated the value of D_{nn} to be 1.4 K for $Ho_2Ti_2O_7$. The reported value of J_{nn}/D_{nn} for $Ho_2Ti_2O_7$ is -0.22 [60]. Using the same value for J_{nn}/D_{nn} ratio, any increase in D_{nn} will result in a more negative value of $J_{nn.}$ In this case of $Ho_2Ge_xTi_{2-x}O_7$ system, D_{nn} is ~2.27 (>1.4 K),

this leads to a more negative value of J_{nn}. This is reflected in the reduction of θ_{cw} with increasing chemical pressure which indicates an increase in a magnitude of J_{nn} (with a negative sign). The positive chemical pressure in $Ho_2Ge_xTi_{2-x}O_7$ shifts the system towards the AFM phase boundary in the phase diagram proposed by *Hertog et al.*[26].

3.3.2 Field dependent magnetization

Figure 3.8 shows the field dependence of the magnetization (M-H) for $Ho_2Ge_xTi_{2-x}O_7$ samples a t 2 K. M_{max} for $Ho_2Ti_2O_7$ is $5.003\mu_B/Ho^{3+}$ consistent with the values previously reported for this material. The value is almost constant for x= 0.0, 0.1, and 0.15 but decreases to $4.23\mu_B/Ho^{3+}$with increase in x to 0.25 possibly due to the sudden decrease in the lattice parameter. The obtained value is half of the actual magnetic moment of Ho^{3+} (10 μ_B) due to the angular averaging of the powdered sample [27].

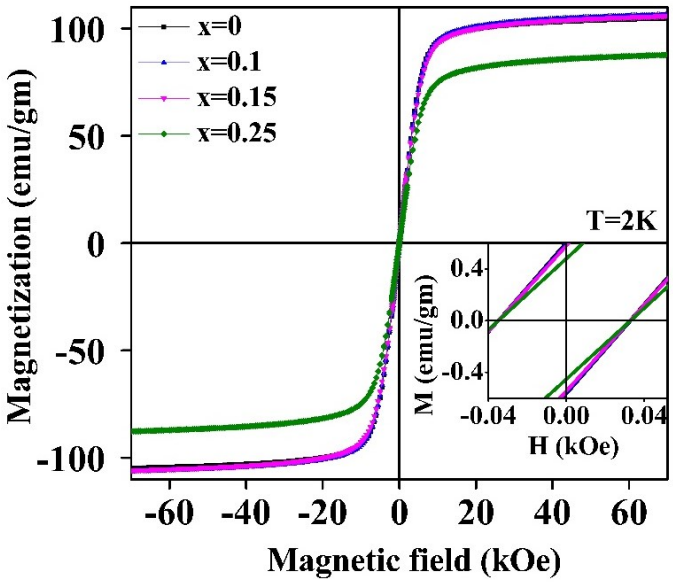

Figure 3.8 Magnetic field dependence of magnetization of $Ho_2Ge_xTi_{2-x}O_7$ (x = 0, 0.1, 0.15 and 0.25) at T = 2 K for H (magnetic field) ranging from -70 to 70 kOe.

3.3.3 Temperature dependent ac-susceptibility

The spin dynamics, when faster or slower than the experimental time scale, will not be detected through dc-susceptibility. Hence the ac-susceptibility measurements were performed for the $Ho_2Ge_xTi_{2-x}O_7$ sample series.

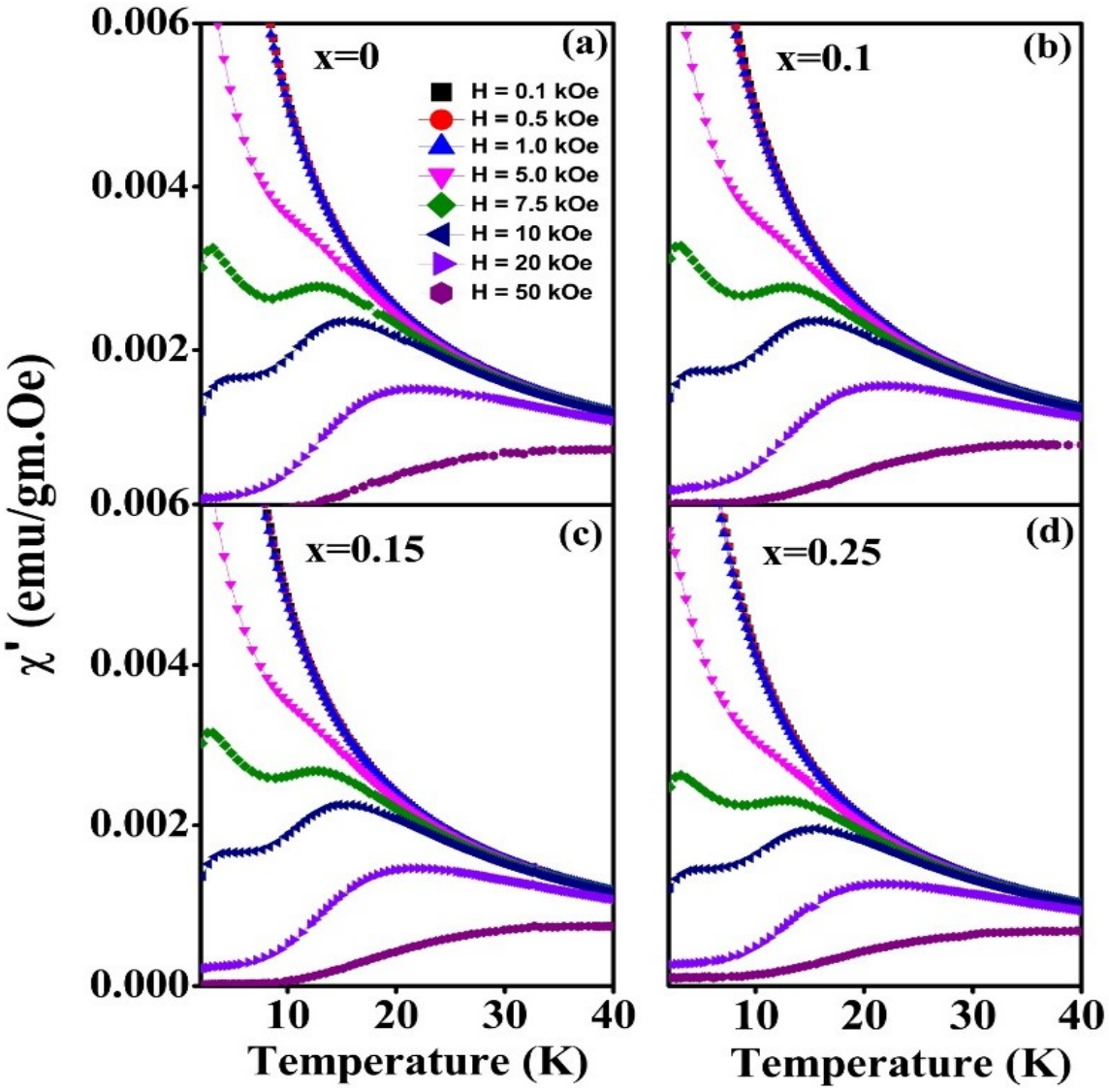

Figure 3.9 Real part of ac-susceptibility of $Ho_2Ge_xTi_{2-x}O_7$ for (a) x = 0 (b) x= 0.1 (c) x= 0.15 (d) x= 0.25 measured at H = 0.1, 0.5, 1, 5, 7.5, 10, 20 and 50 kOe at an applied ac-frequency of 500 Hz.

Figure 3.9 shows the real part of the ac-susceptibility of $Ho_2Ge_xTi_{2-x}O_7$ (x = 0, 0.1, 0.15 and 0.25). The ac-susceptibility measurement, in the absence of any applied dc-magnetic field, shows a canonical paramagnetic behavior for each composition. Hence, the data has been further collected at an applied dc magnetic field of 0.1, 0.5, 1, 5, 7.5, 10, 20, and 50 kOe. For $Ho_2Ge_xTi_{2-x}O_7$ (x = 0, 0.1, 0.15, and 0.25) absence of any signs of spin relaxation in ac-susceptibility data indicates no response of spin dynamics to the applied dc-magnetic field till 1 kOe. However, with further increase in the magnetic field's intensity, two prominent features corresponding to spin freezings appear. An increase in the magnetic field intensity from 0.1 kOe to 5 kOe initiates the appearance of a thermally activated high temperature (~ 15 K) relaxation feature, which corresponds to single ion spin freezing. With an increase in the magnetic field to 7.5 kOe, freezing corresponding to spin ice state emerges at 3.2 K (T_{ice}) along with the pronounced appearance of single ion freezing temperature (T_s) at 13.02 K. These two different spin freezing corresponds to two different time (relaxation time τ_0) and energy scale (Arrhenius energy) for spin flipping having two different origins. Single ion spin freezing becomes more prominent with a further increase in the applied dc magnetic field of 10 kOe. Both spin ice freezing and single ion spin relaxation shifts towards the higher temperature side to 4.07 K and 14.87 K, respectively. The peak corresponding to spin ice freezing (T_{ice}) disappears with further increase in the magnetic field to 20 kOe, and single ion freezing further shifts towards the higher temperature side (20.66 K) for $Ho_2Ti_2O_7$.

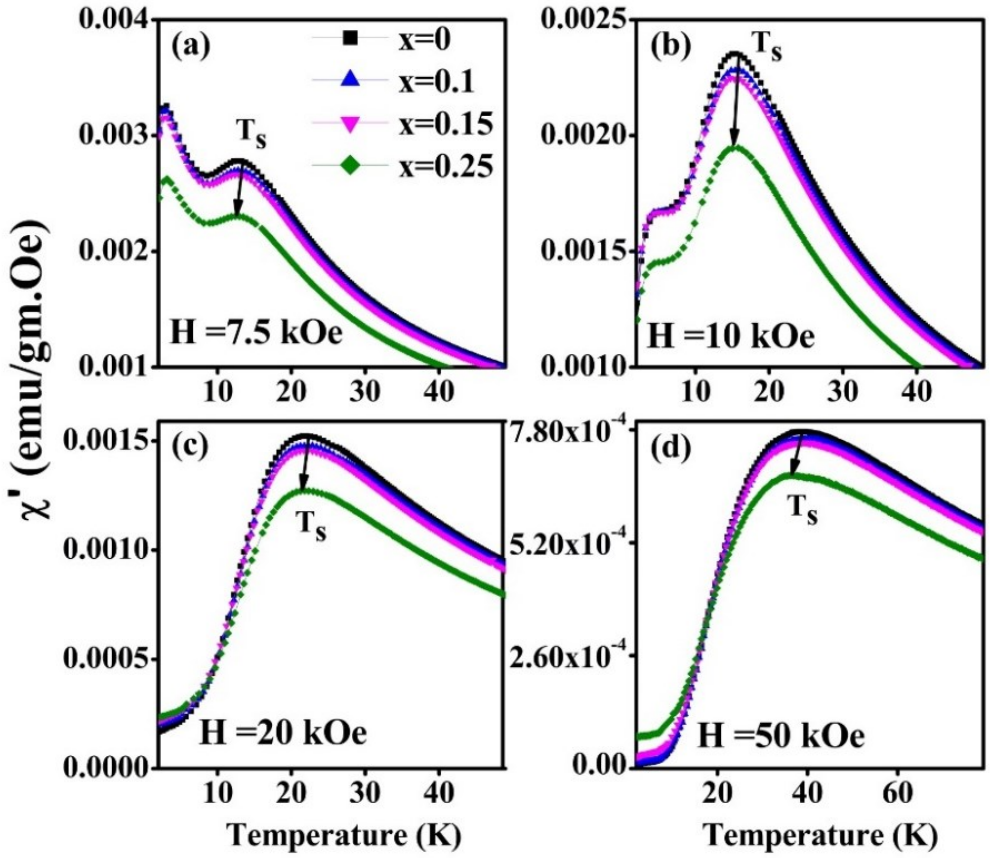

Figure 3.10 Variation of ac susceptibility with temperature for $Ho_2Ge_xTi_{2-x}O_7$ (x = 0, 0.1, 0.15 and 0.25) for an applied field of (a) H = 7.5 kOe (b) H = 10 kOe (c) H = 20 kOe (d) H = 50 kOe at 500 Hz. Single ion freezing temperature (T_s) is shifted towards the low lower temperature with increasing chemical pressure effect.

To understand the role of chemical pressure upon the spin dynamics, composition dependent ac-susceptibility response of $Ho_2Ge_xTi_{2-x}O_7$ (x = 0, 0.1, 0.15 and 0.25) were analyzed as shown in the **Figure 3.10**. Single ion spin freezing (T_s) shifts towards lower temperature side with an increase in x for a given frequency of 500 Hz. However, we observe no frequency dependence (till ν =700 Hz) with increasing chemical pressure in $Ho_2Ge_xTi_{2-x}O_7$ (x = 0, 0.1, 0.15 and 0.25) as shown in **Figure 3.11** for fixed applied magnetic field of 7.5 kOe.

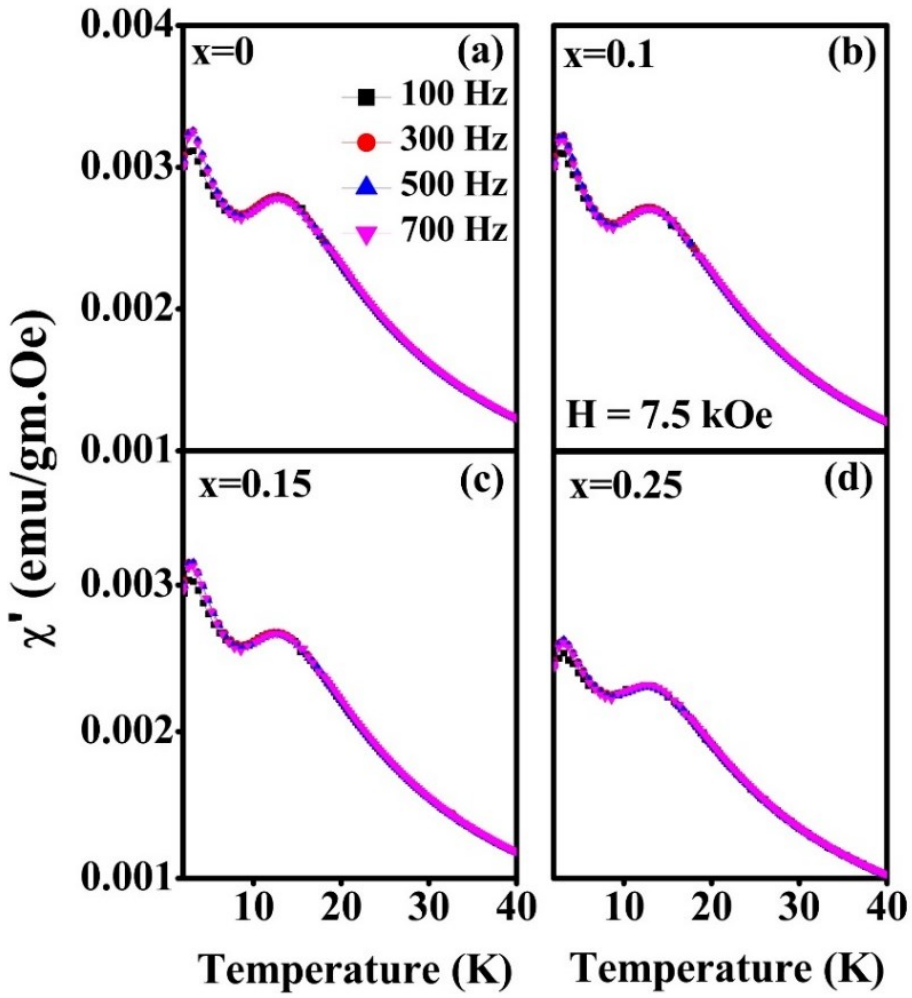

Figure 3.11 Frequency independence of ac susceptibility of $Ho_2Ge_xTi_{2-x}O_7$ for (a) x = 0 (b) x= 0.1 (c) x= 0.15 (d) x= 0.25 for applied dc magnetic field H = 7.5 kOe.

The variation of T_s with the external applied magnetic field for $Ho_2Ge_xTi_{2-x}O_7$ is also shown in **Figure 3.12**. The evolution of single ion freezing temperature (T_s) with x in $Ho_2Ge_xTi_{2-x}O_7$ for different applied magnetic fields is shown in **Figure 3.13.**

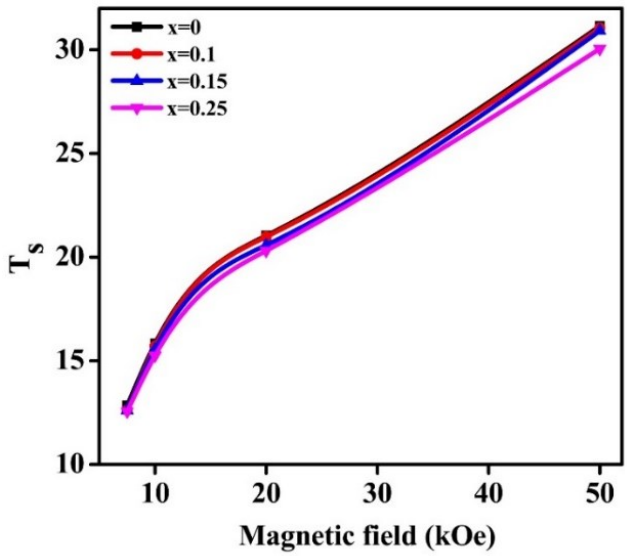

Figure 3.12 Shift in the single ion freezing temperature (T_s) against external applied magnetic field for $Ho_2Ge_xTi_{2-x}O_7$ (x = 0, 0.1, 0.15 and 0.25) system.

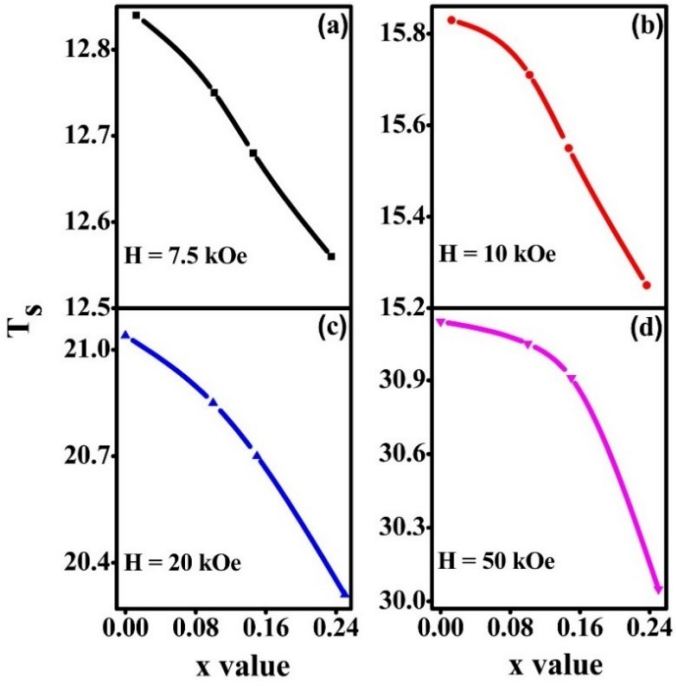

Figure 3.13 Variation of single ion freezing temperature (Ts) with composition in $Ho_2Ge_xTi_{2-x}O_7$ (x value = 0, 0.1, 0.15 and 0.25) at an applied magnetic field of (a) H = 7.5 kOe (b) H = 10 kOe (c) H = 20 kOe (d) H = 50 kOe for an applied frequency of 500 Hz.

Shift of T_s towards higher temperature indicates increasing energy barrier to spin relaxation with the increase in the applied magnetic field similar to $Dy_2Ti_2O_7$ spin ice [83]. The effect of the chemical pressure effect on T_s is discussed in detail in next section. Feature corresponding to spin ice freezing (T_{ice}) in ac-susceptibility data flattens with the increase in the magnetic field to 10 kOe for $T < T_s$. With increasing applied dc magnetic field of 20 kOe, both T_{ice} and T_s merges in a single hump-like feature due to shift of T_{ice} to a higher temperature. The broadened peak for T_s for the applied field of 20 kOe, in comparison with the same for 10 kOe indicates the shift of T_{ice} rather than its disappearance. The single-ion spin freezing $T_s \sim 15$ K, occurs through the spin-flip relaxation along the [111] axial directions without any correlation with their neighbours [84]. Spin ice freezing (T_{ice}) remains unaffected with the increase in chemical pressure, the more clear picture is given in **Figure 3.14.**

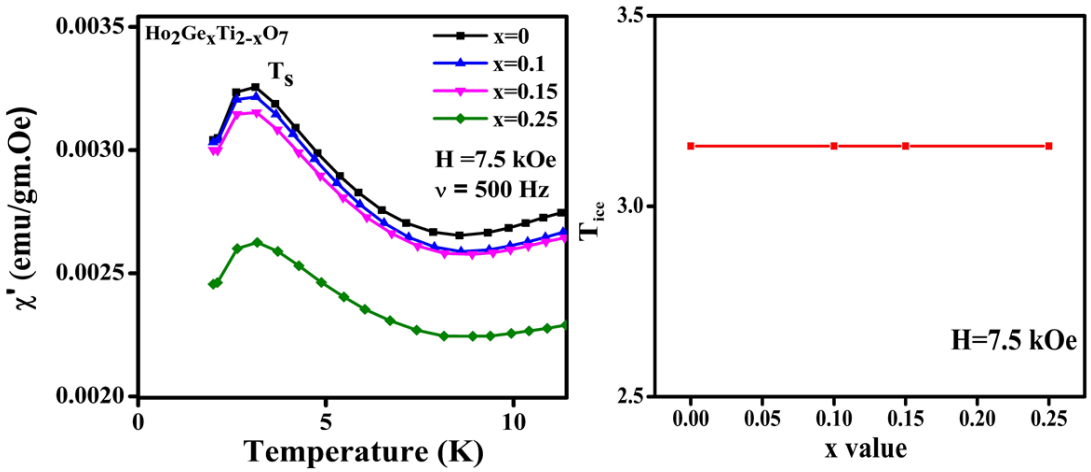

Figure 3.14 Spin ice freezing (T_{ice}) remains unaffected with the increase in chemical pressure for $Ho_2Ge_xTi_{2-x}O_7$ (x = 0, 0.1, 0.15 and 0.25) system.

Spin ice freezing below 4 K is correlated with the occurrence of mean-field, which splits the Ho^{3+} ground state (Zeeman splitting). This mean-field development is due to the formation of the ice like spins orientation at the vertex of tetrahedra below 4 K. These spins define the

vector field of flux lines on the tetrahedral lattice, which is divergence-free due to 2 in - 2 out ice rule. The spin vectors represent an artificial magnetic field B as shown in **Figure 1.23 (a)** [37]. This field posses a fluctuating nature because of disorderliness in spins, which lifts the degeneracy of Ho^{3+} ground-state doublet $|\pm M_j>$, $M_j=8$ [36]. The transverse component of this fluctuating field mixes the higher $|M_j>$ states with $|\pm 8>$ ground state doublet providing a number of degenerate spin configurations as described in chapter 1. Hence, the T_{ice} spin relaxation feature remains unaltered with the increase in chemical pressure. It establishes the robustness of spin ice freezing against induced chemical pressure. A similar observation has been made for $Dy_2Ti_2O_7$ spin ice where no breaking of the ice rule is observed with magnetic dilution at the Dy site [61]. Thus the majority of the spins in the $Ho_2Ge_xTi_{2-x}O_7$ system still follow an "ice-like" configuration even after the applications of chemical pressure and subsequent changes in subtle atomic arrangements.

The dominance of the crystal field (CF) comes into the picture at T ~ 15 K. The frequency dependence of this single ion spin relaxation feature provides the value of activation energy (E_a) of the first excited crystal field level of Ho^{3+} to be ~ 20.6 meV (≡ 240K). At T~15 K, CF confines the spins to a double-well potential of depth, which is the barrier height of the first excited crystal field level of Ho^{3+} single ion. Below 15 K, which is much less than the barrier height of 240K, the classical barrier is invincible, and hence spin relaxation occurs through the quantum mechanical tunneling phenomenon as quasi-classical spin relaxation channels are exhausted below T (~ 15 K) [85]. T_s (~ 15 K) shifts towards lower temperature with an increase in chemical pressure, as could be seen from **Figure 3.13.** It indicates a change in activation energy (~ 20.6 meV) corresponding to single ion freezing due to alteration in the first excited crystal field level of $Ho_2Ti_2O_7$. The strong crystal field anisotropy is subjected

by the O' oxygen ligand, which is transverse to the antiprismatic arrangement of six oxygen (O) atoms. This effect aligns the spin (parallel or anti-parallel) along [111] direction, spins being arranged at the tetrahedral corner following "all in all-out", "3 in - 1 out" or "3 out - 1 in" configuration. Single ion crystal field spectrum is expressed in terms of quantum number |J, Mj>, Mj being the projection of correlated 4f electrons along |111> axis. The decrease in the bond angle of O-Ho-O' suggests that increased chemical pressure possibly makes a difference in the projection of spins along the [111] axis. The interaction between magnetic rare-earth Ho^{3+} and its crystalline environment is also expressed through simple Hamiltonian as

$$H_{CF} = -\sum |e_i| V_{CF}(r_i) \quad (3.3)$$

where V_{CF} is the crystal field potential acting on the f electrons of the Ho^{+3} ion from surrounding ions (O^{2-}) [58]. The i_{th} electron of Ho^{3+} feels a potential $V_{CF}(r_i) = V_{CF}(r_i,\theta_i,\varphi_i)$, which is having both positional and angular dependence on surrounding ligand ions. A decrease in Ho-O' and Ho-O bond angle and O-Ho-O' bond angle with increasing chemical pressure changes the antiprismatic character of the pyrochlore structure imposed by trigonal D_{3d} symmetry of Ho^{3+} ion. Hence the variation of the crystallographic parameter in $Ho_2Ge_xTi_{2-x}O_7$ earlier listed in **Table 3.2** substantiates the alteration in CF Hamiltonian responsible for the shift in single ion freezing (T_s) in the $Ho_2Ge_xTi_{2-x}O_7$ system.

Crystal field splitting depends upon the overlapping extent of Ho^{3+} 4f and O'^{2-} 2p orbital. An increase in the crystal field splitting as both the linear and angular separation between Ho^{3+} and O'^{2-} decreases with an increase in chemical pressure is expected. Hence, it is naively expected further that increase in CF splitting of Ho^{3+} must enhance the associated energy barrier for the first excited crystal field level ($E_a \sim 20.6$ meV), and hence T_s must be shifted

towards its higher temperature side [61]. However, the suppression of T_s towards the lower temperature side in the $Ho_2Ge_xTi_{2-x}O_7$ system indicates the contribution of another factor. It advocates the crystal field-phonon coupling emerging at $T \sim T_s$, which lowers the energy scale for the first excited state of the Ho^{3+} ion, the evidence of which is given in next section.

3.4 Low temperature SRXRD measurement for $Ho_2Ge_{0.1}Ti_{1.9}O_7$

Crystal field phonon coupling is established through the variation of lattice volume with temperature between (15-150) K for x=0.1 in $Ho_2Ge_xTi_{2-x}O_7$ through SXRD measurement.

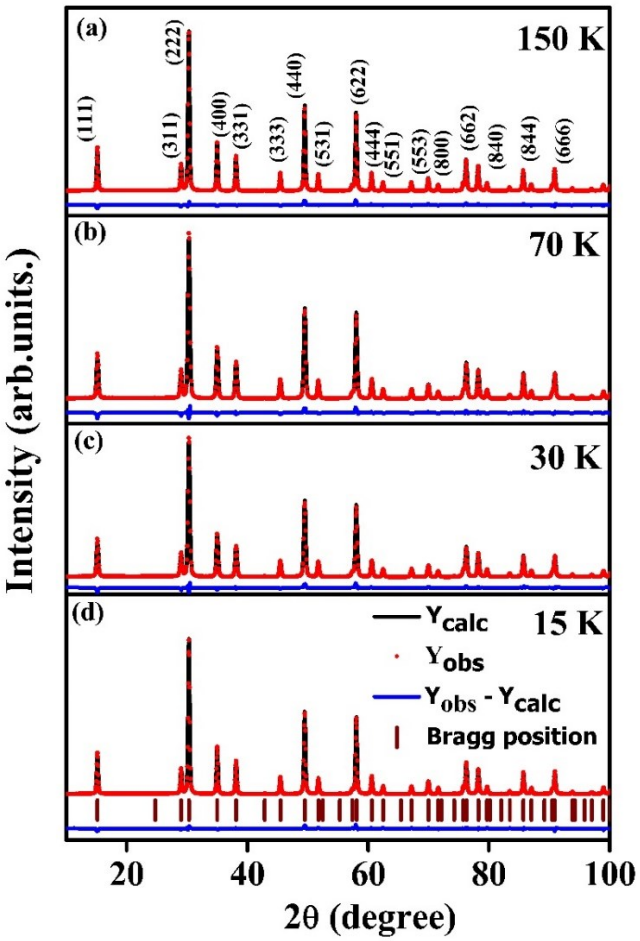

Figure 3.15 Low temperature synchrotron x-ray diffraction pattern of $Ho_2Ge_xTi_{2-x}O_7$ (x = 0.1) at (a) T=150 K, (b) T= 70 K, (c) T=30 K (d) T=15 K.

Figure 3.15 shows its selected low-temperature SXRD pattern for T = 150, 70, 30, and 15 K, and it's Rietveld refinement. The obtained value of lattice volume was plotted against temperature. Lattice volume decreases linearly till 30 K, below which it shows an anomalous increment. It indicates that till 30 K thermal effect (phonon) is responsible for the reduction in lattice volume. The possible explanation for abrupt increment below 30 K is the dominance of CF effect over lattice vibration at 30 K. This behavior in lattice volume establishes crystal field phonon coupling in $Ho_2Ge_xTi_{2-x}O_7$ system below 30 K.

3.5 Crystal field-phonon coupling

To further confirm this coupling, the Debye-Grüneisen equation was used to fit the change in unit cell volume against temperature for x = 0.1, as shown in **Figure 3.16.**

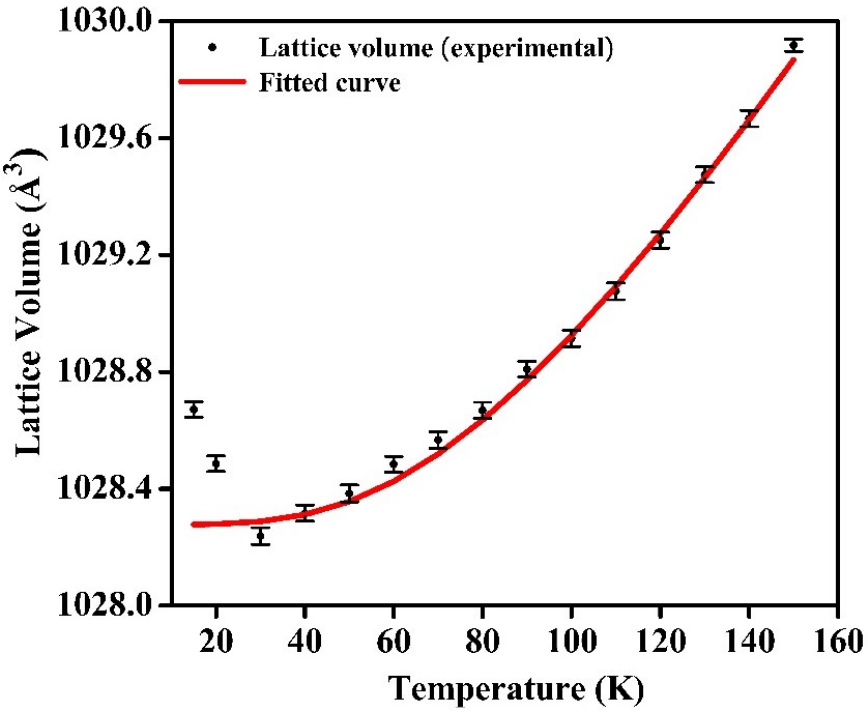

Figure 3.16 Debye Grüneisen fit of $Ho_2Ge_xTi_{2-x}O_7$ (x = 0.1) indicating the deviation from its linear behavior below 30 K.

The equation is as follows:

$$V \cong V\,(T=0) + \int_0^T \frac{\gamma C_v}{B}\,dT$$

$$\cong V\,(T=0) + \frac{9\gamma N k_B}{B} T \left(\frac{T}{\Theta_D}\right)^3 \int_0^{\Theta_D/T} \frac{e^x}{e^x - 1} dx \qquad (3.4)$$

V (T=0), Θ_D and $9\gamma Nk_B/B$ are fitting parameters; *V (T = 0)* represents the lattice volume at 0 K, Θ_D is the Debye temperature, γ is Grüneisen parameter and B is the bulk modulus. The solid line shows the fitted curve using the above function. The said equation accounts only the thermal expansion (phonon contributions) in solids due to the presence of anharmonic parts of lattice vibration. The fitted curve does not account the data points below 30 K, indicating that the change in lattice volume below 30 K is not of entirely thermal origin. Hence, the CF effect's dominance below 30 K could be responsible for this distinct low-temperature behaviour [86]. Similar behaviour in thermal expansion has also been observed in $Ho_2Ti_2O_7$ spin ice system using SXRD measurement [17]. A possible multipolar phase spontaneously breaking of rotational symmetry while preserving translational invariance has been reported in case of $Cd_2Re_2O_7$ pyrochlore near 200 kelvin [87]. Such a electronic phase transition coupled with the strong spin-orbit coupling can not be ignored in this case as well through the dominance of CF below 30K.

Similar variation of lattice constant (along both a and c directions) at low temperature (below 160 K) has been manifested in $SrRuO_3$ system as shown in **Figure 3.17** (Debye temperature = 526 K) too though similar system $CaRuO_3$ (Debye temperature = 542 K) does not exhibit such anomaly.The thermal response of system of $CaRuO_3$ followed the Debye function down to the lowest temperature which indicates entirely the phonon contribution. This behaviour has been reported by T. Kiyama et al [86].The anomaly in the variation of temperature

dependence against the volume function for $SrRuO_3$ indicates that thermal expansion is affected by another factor beside lattice vibration.

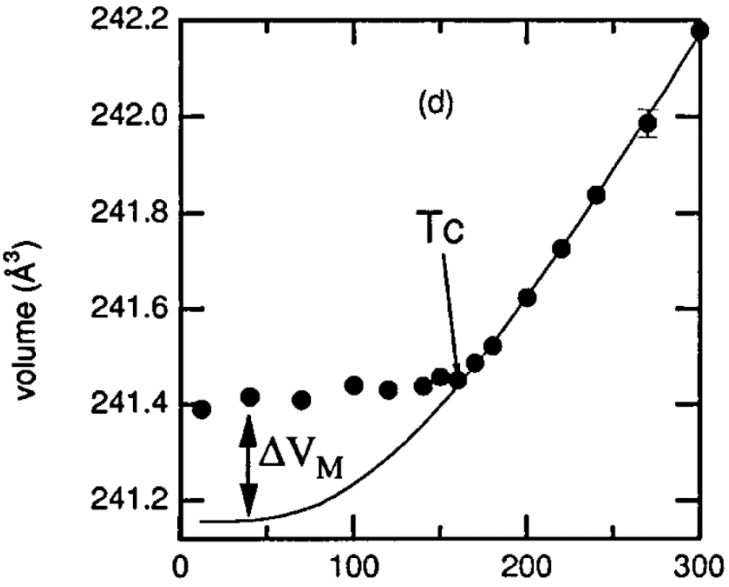

Figure 3.17 Temperature dependence of the unit-cell volume of $SrRuO_3$. The solid line represents the contribution of the phonon fitted using the Debye function. [86]

In this system, another factor attributed is ferromagnetism since the anomaly just aroused at the Curie-Weiss temperature. Since in our system it has been reported that strong crystal electric field responsible for single ion freezing comes into picture at (E_a~240 K (20.6 meV)) but its dominance is seen at T_s ~ 30 K. It could be seen in the form of spin relaxation feature exhibited in the ac susceptibility curve. These observations strongly indicates crystal field coupling in $Ho_2Ge_xTi_{2-x}O_7$ system.

3.6 Conclusions

The magnetic ordering and spin dynamics in the $Ho_2Ge_xTi_{2-x}O_7$ frustrated magnetic system. Antiferromagnetic exchange interaction, J_{nn} controls the spin dynamics effectively (more sensitive to structural distortion) since an almost similar value of the dipolar coupling constant

with an increase in x in $Ho_2Ge_xTi_{2-x}O_7$ has been obtained. The chemical pressure induced in the $Ho_2Ti_2O_7$ matrix leaves the spin ice feature unaffected, whereas it alters the single ion crystal field spectrum of Ho^{3+}. The evolution of single ion freezing temperature (T_s) with chemical pressure is attributed to the alteration in the crystal field spectrum, i.e., lowering the first excited crystal field state of Ho^{3+}. The change in crystal field level is attributed to crystal field-phonon coupling. Tunneling dynamics at T_{ice} is its intrinsic consequence because of geometrical frustration. $Ho_2Ge_xTi_{2-x}O_7$ pyrochlore magnetic materials constitute a new class of robust spin ice system. The other end of the $Ho_2Ge_xTi_{2-x}O_7$ towards germanate side will now be disscussed in the next chapter.